www.czasopisma.pan.pl PAN POLSKA AKADEMIA NAUK www.journals.pan.pl

Arch. Metall. Mater. **67** (2022), 3, 889-900

DOI: https://doi.org/10.24425/amm.2022.139680

LEVENT ELEN[1*], YUNUS TUREN[2], HAYRETTIN AHLATCI[2], YAVUZ SUN[2], MEHMET UNAL[3]

INVESTIGATION OF MICROSTRUCTURE, MECHANICAL AND CORROSION PROPERTIES OF BIODEGRADABLE Mg-Ag ALLOYS

In this study, microstructure, mechanical, corrosion and corrosive wear properties of Mg-xAg the as-cast and extruded alloys (x: 1, 3 and 5 wt. % Ag) were investigated. According to the experimental results, as the amount of Ag added in the casting alloys increases, the secondary phases (Mg_4Ag, $Mg_{54}Ag_{17}$) emerging in the structure have become more clarified. Furthermore, it was observed that as the amount of Ag increased, the grain size decreased and thus the mechanical properties of the alloys increased. Similarly, the extrusion process enabled the grains to be refined and the mechanical properties to be increased. As a result of the in vitro tests performed, the Mg-1Ag exhibited very bad corrosion properties compared to other alloys. On the other hand, according to corrosive wear tests results, a high wear rate and friction coefficient were found for Mg-5Ag alloys.

Keywords: Mg-Ag alloys; biodegradable; mechanical properties; microstructure properties; corrosion

1. Introduction

Although the most common materials for the production of biodegradable implants are polymers, Mg-based alloys have been an increasing interest focus in medical fields such as [1-3] as a better biodegradable material for load-bearing applications due to their superior strength and ductility combinations. Magnesium is potentially a great implant material because it is not toxic to the human body in moderate amounts. Mg^{2+} is abundant in the human body and takes an active role in many metabolic reactions and biological mechanisms [4]. Furthermore, the Young's modulus of magnesium (41-45 GPa) is closer to the natural bone (3-20 GPa) than that of iron (~211.4 GPa) [5,6].

Incompatibility of Young's moduli between bone and metallic implant materials might cause critical clinical problems such as implant loosening, injury at healing process, skeletal thickening, and chronic inflammation [7-9].

Thus, the biocompatibility and biodegradation tendency of magnesium in the human body has made magnesium alloys a potential candidate for biodegradable implant applications [5,10]. However, this is only effective when the corrosion properties can be controlled. Because today, the biggest disadvantage of magnesium alloys as implant materials is that they corrode very quickly [11], this is because the Pilling-Bedworth (PB) ratio of 0.84 for the oxide layer (MgO) is less than 1 and the oxide layer cannot form a stable protection [12]. Since Mg is a passive metal, pitting corrosion will occur at the free corrosion potential when exposed to chloride ions in a non-oxidizing corrosive environment [13]. These emerging corrosion pits are first observed in defects located adjacent to the secondary phase particle boundaries as a result of the deterioration of passivity [13]. This is then followed by the formation of an electrolyte cell in which the secondary phase particles act as the cathode and the surrounding Mg main matrix as the anode. As a result, these reactions, which start with an anodic reaction, then continue with a series of autocatalytic reactions and form pitting corrosion. This case emerges as an important factor that increases the corrosion rate of Mg [14]. Therefore, there are several studies in the literature regarding the corrosion control of Mg. (Koc) [15], revealed that the corrosion of magnesium can be controlled by the addition of certain amounts of Zn. By (Kara at al.) [16], suggested that the corrosion resistance of magnesium alloys can be controlled by microstructure properties such as grain size or secondary phases. It has also been proven by some studies [17-20] that it has an

[1] KARABUK UNIVERSITY, TOBB VOCATIONAL SCHOOL OF TECHNICAL SCIENCES, MACHINERY AND METAL TECHNOLOGIES DEPARTMENT, KARABUK, TURKEY
[2] KARABUK UNIVERSITY, METALLURGICAL AND MATERIALS ENGINEERING, FACULTY OF ENGINEERING, TURKEY
[3] KARABUK UNIVERSITY, MANUFACTURING ENGINEERING, TECHNOLOGY FACULTY, TURKEY

* Corresponding author: leventelen@karabuk.edu.tr

© 2022. The Author(s). This is an open-access article distributed under the terms of the Creative Commons Attribution-NonCommercial License (CC BY-NC 4.0, https://creativecommons.org/licenses/by-nc/4.0/deed.en which permits the use, redistribution of the material in any medium or format, transforming and building upon the material, provided that the article is properly cited, the use is noncommercial, and no modifications or adaptations are made.

important role in the development of microstructure control Mg alloys. (Zengin at al.) [21], emphasized that the Sn element improves the corrosion properties of Mg alloys. However, since the fluids in the human body create an environment with pH levels between 1-9, the mechanical properties of biomaterials should be good as well as their corrosion properties.

Although it has high solubility (15% by weight) in magnesium, silver (Ag) [22], which develops the mechanical properties of magnesium alloys by forming solid solution, is a very important element in the field of biomaterials. The main reason why it is an important element in the field of biomaterials is that it shows antibacterial behavior by deforming the DNA and RNA structure of bacteria and preventing them from multiplying and surviving [23]. Magnesium alloys with Ag addition are the most ideal alloys to reduce and eliminate the viability of facultative anaerobic, spore and gram-positive bacteria, especially methicillin-resistant staphylococcus aureus (MRSA, a type of bacteria that lives and grows in general mucosal tissues) [23]. (Hardes at al.) and (Bosetti at al.), reported that in addition to antibacterial capability, small amounts of Ag content in alloys or coatings also significantly increased cytocompatibility [24] and cell viability [24,25]. Ag in any form was considered non-toxic [26] and non-carcinogenic to the immune, cardiovascular, nervous, and reproductive systems [27]. Thus, the use of Ag in the healthcare field has become quite common in recent years.

Therefore, in this study, the microstructure, mechanical and in vitro corrosion properties of (1 wt. %, 3 wt. % and 5 wt. %) Ag containing Mg-Ag alloys in hanks solution were investigated.

2. Materials and methods

In the experimental studies, 99.9% pure Mg as matrix materials and 99.9% pure Ag as alloying elements supported by BDM Bilginoglu company and 4D Machine and Technology respectively.

An atmosphere-controlled induction furnace is used in the melting processes of the investigated alloys. Following the melting and mixing processes, the melting was casted in steel mold under gas (CO_2 + 1% SF_6) protection by gravity casting method. The casting temperature and the mold temperature set on at 750°C and as 250°C respectively.

Chemical compositions of the produced Mg-Ag alloys after casting were determined by using the XRF (X-Ray Fluorescence) method using Rigaku ZSX Primus II brand device.

After the casting process, homogenization annealing was applied at 430°C for 12 hours in order to eliminate possible defects such as small amounts of segregation, inhomogeneous grain size and distribution in cast parts. The extrusion process was carried out at 16:1 extrusion ratio, 300°C temperature and 1 mm/s constant extrusion speed.

Microstructure investigations were carried out by Nikon Epiphot 200 brand optical microscope (OM) and Carl Zeiss Ultra Plus brand scanning electron microscopy (SEM). Before the microstructure characterizations, the samples were etched with picric acid solution.

Formed phases in microstructure were characterized by Rigaku Ultima IV x-ray diffractometer (XRD) with a scanning speed of 3 deg/min and a scanning angle from 10° to 90°.

Tensile tests of the cast and after the extrusion specimens were carried out on a Zwick/Roell Z600 tensile device at a tensile speed of 1.67×10^{-3} mm/s^{-1}. In the tensile test, at least five samples were prepared for the each alloys. The hardness of the samples were determined by the Vickers hardness (Vickers-Qness60A) test under 0.3 kg load.

Characterization of corrosion properties of the cast and extruded samples was carried out at ~37°C, pH 7.4. In Hanks solution consisting of its composition: NaCl 8.0 g/l, KCl 0.4 g/l, $CaCl_2$ 0.14 g/l, $NaHCO_3$ 0.35 g/l, $C_6H_6O_6$ (glucose) 1.0 g/l, $MgCl_2$ $6H_2O$ 0.1 g/l, $MgSO_4$ $7H_2O$ 0.06 g/l, KH_2PO_4 0.06 g/l, Na_2HPO_4 $12H_2O$ 0.06 g/l. For the immersion corrosion test, 8 mm diameter and 10 mm long specimens were cut from the cast and extruded alloys. The samples were ground with 120-1200 SiC abrasive papers and cleaned with ethyl alcohol in an ultrasonic bath for 5 minutes prior to testing. Each sample was weighed (M_s) and its surface area was measured before starting the test and then immersed in corrosive medium for 24 hours. Immersion tests were repeated three times. After each test, the corrosion products of the samples were cleaned by immersion in 182 g l^{-1} aqueous chromic acid solution in an ultrasonic cleaner for 5 minutes. It was then washed with deionized water and placed in an ultrasonic bath in ethyl alcohol for 3 minutes. Finally, it was dried in warm air and then the mass (M_f) was weighed. The difference between the first measurement (M_s) and the last measurement (M_f) is determined as the corrosion mass loss.

The mean corrosion rate CR_m was determined by using following equation:

$$CR_m = \frac{8.76\times10^4\times\Delta g}{A\times t\times\rho} \tag{1}$$

where Δg is the weight change (difference before and after immersion) in grams, A is the surface area of the sample in cm^2, t is the immersion time in hours and ρ is the density in g/cm^3.

Pitting factor is calculated by the ratio between P_{corr} (maximum penetration depth) and the average penetration depth obtained by dividing W_{corr} (weight-loss corrosion rate) with the density [28].

Electrochemical measurements were made at ~37°C, in Hanks solution with 7.4 pH, with Gamry model PC4/300 mA potentiostat/galvanostat with computer controlled DC105 corrosion analysis. The tests were repeated five times. Polarization curves were constructed starting from –0.25 V (open circuit potential versus Eoc) to +0.25 V (Eoc versus) at a scan rate of 1 mVs^{-1}. Using a sample with 0.25 cm^2 open area as the working electrode, a graphite rod as counter electrode and a saturated calomel electrode (SCE) as a reference electrode, tafel curves were drawn and the corrosion potential (E_{corr}) and corrosion current density (I_{corr}) were recorded.

Wear tests of the cast and extrusion specimens were measured in a reciprocating wear tester, in Hanks solution, under constant load, at constant speed and at a constant distance. Tests were carried out under 20 N load, 0.1 m/s sliding speed and 400 m sliding distance in total. Before the abrasion test, the samples were cut to fit the sample bed in the device and their surfaces were sanded up to 1200 numbered sandpaper and cleaned with alcohol. During abrasion, the friction force was measured by the load cell connected to the tribometer arm and recorded in the computer instantly. AISI 52100 quality high hardness steel ball is used as the indenter material.

3. Results and discussion

Chemical compositions analysis results of the produced casting Mg-Ag alloys are given in TABLE 1.

TABLE 1

The compositions by weight in the investigated Mg-Ag alloys

Alloys	Alloy Code	Elements (% wt.)					
		Ag	Al	Si	Ca	Mn	Mg
Pure Mg	Q0	—	—	—	—	—	99,9
Mg-1Ag	Q1	1,08	0,02	0,04	0,01	0,02	Balance
Mg-3Ag	Q3	3,35	0,02	0,03	0,01	0,02	Balance
Mg-5Ag	Q5	5,4	—	—	0,03	0,03	Balance

XRD phase analysis results of Mg-Ag alloys are given in Fig. 1. According to these results, the presence of Mg_4Ag and $Mg_{54}Ag_{17}$ phases in addition to the α-Mg main matrix were determined in the microstructure. Furthermore, it has been assessed that the Mg_4Ag phase is more dominant in the magnesium-rich regions and the other secondary phases do not exhibit a visible situation. This situation has also been reported in the literature [23,29].

Optical microscope images of the investigated Mg-Ag alloys are shown in Fig. 2. The microstructure examinations of the cast

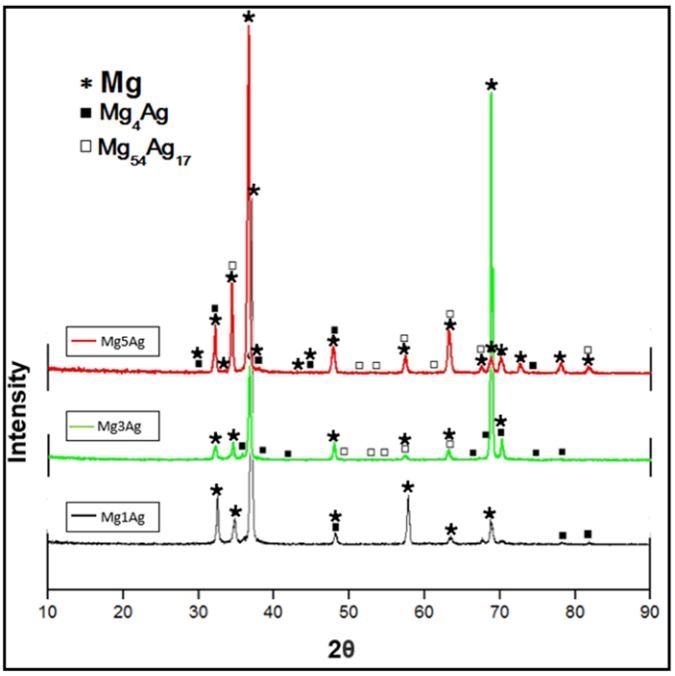

Fig. 1. XRD analysis of Mg-Ag alloys

Mg-Ag alloys reveal that the secondary was observed that the secondary dendrites in the grain [30] increased significantly with the increase of Ag content and that the eutectic phases formed during solidification [31] were dispersed along the grain boundaries [30]. It was also found that the grain size decreased with increasing Ag content. In addition, the grain size was reduced through the elimination of secondary dendrite particle by hot extrusion [30].

Combined with SEM images and EDX analysis (Fig. 3) indicated that the eutectic consists of large β-Mg_4Ag/$Mg_{54}Ag_{17}$ phase particles and α-Mg phase. Moreover, it was also observed that the secondary phase ($Mg_{54}Ag_{17}$) extends along the extrusion direction [32]. In Fig. 3, while the phases in the form of particles in the direction of extrusion are $Mg_{54}Ag_{17}$, the light colored linear phase with approximately 30% Ag observed at the end of the line analysis is Mg_4Ag.

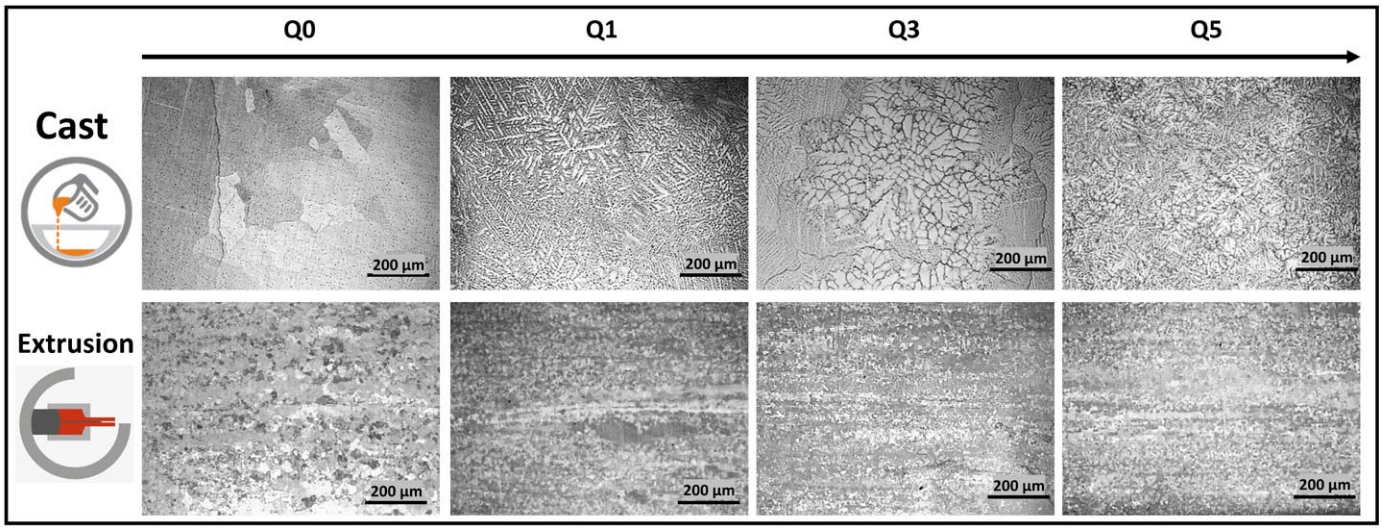

Fig. 2. Optical microscope images of the sections parallel to the casting and extrusion directions of the alloys

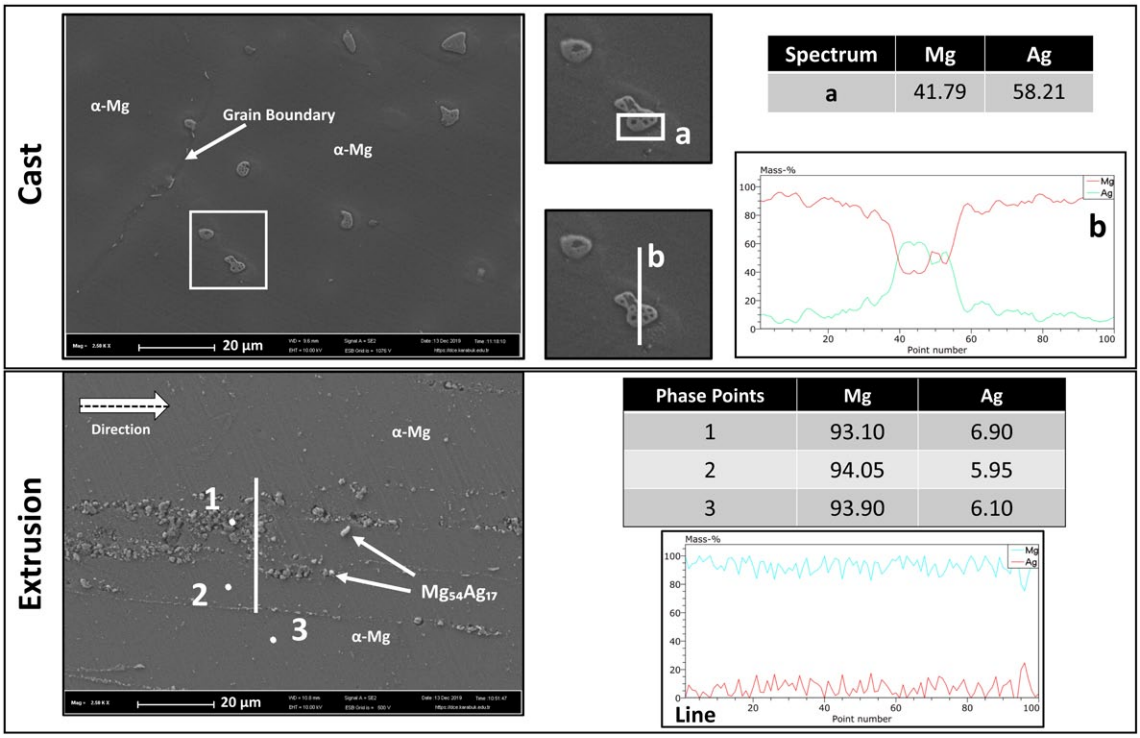

Fig. 3. SEM images and EDX analysis of the alloy Q5

Mechanical properties of the cast alloys are shown in (Fig. 4(a)). Compared to the pure magnesium, it is thought that the grain size decreases with the addition of Ag (Fig. 2) and thus, mechanical properties of the investigated alloys increased with Ag additions. It is thoughted that the mechanical test results confirm this situation. In addition, (Zhao et al.) [33] reported similar results with this study.

The extrusion process of the Mg alloy is a thermomechanical process applied to the material and the extrusion process can be considered as one of the important grain refining techniques. Consequently, it is known that the most important parameters affecting grain refinement in the extrusion process are the working temperature and the extrusion rate. Therefore, in this study, the extrusion rate together with the temperature

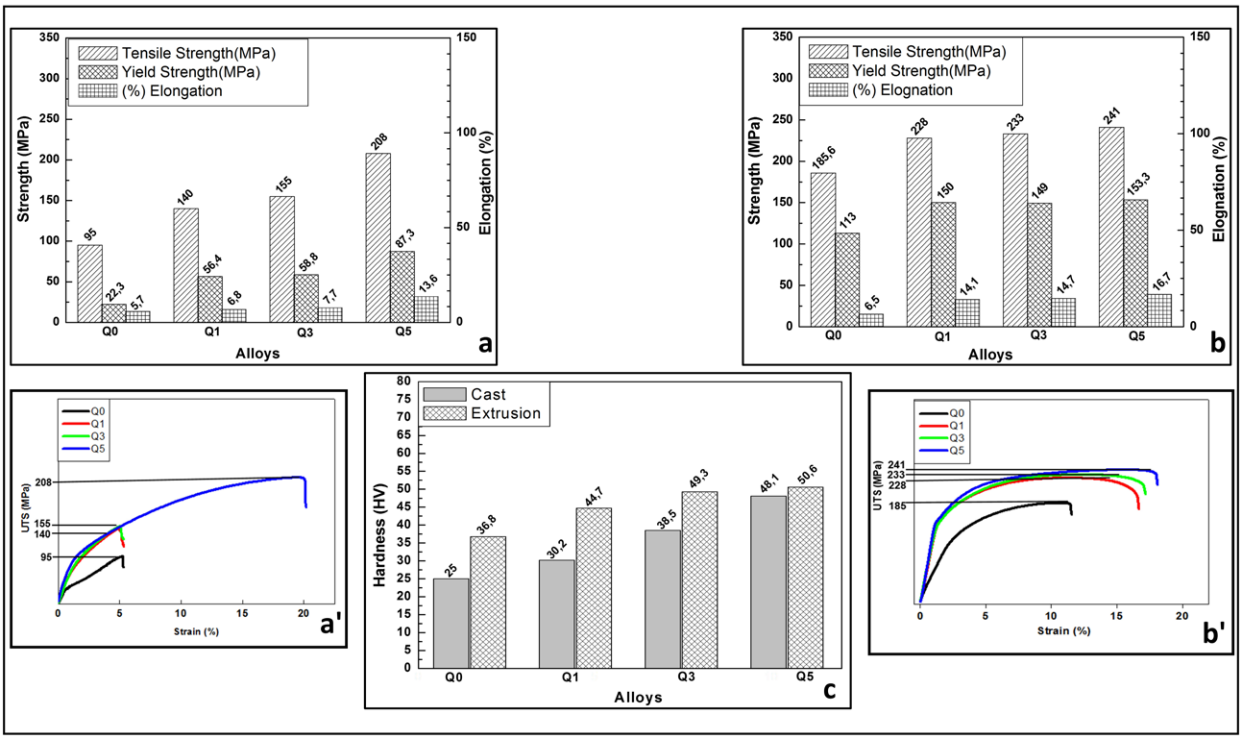

Fig. 4. (a) hardness values, and tensile-yield strength and % elongation values of the (b) cast and (c) extruded alloys with respect to the Ag addition

of the samples and extrusion die was controlled according to the temperature and extrusion rate highlighted in the literature [34-36]. According to the results of the tensile test performed after extrusion, it was observed that the UTS and TYS and % elongation values (Fig. 4(b)) increased due to the grain structure refined by the extrusion process as well as the Ag addition. The influence of the extrusion process on the mechanical properties of the investigated Mg-Ag alloys are agreement to the studies of the Ref [36,37]. Due to the hexagonal close-packed (HCP) crystal structure, the number of simple sliding systems in Mg alloys are not sufficient to provide homogeneous plastic deformation according to Von Mises criteria [38]. For this reason, it is not possible to achieve a fully compatible deformation by the dislocation movement [38]. Instead, it occurs by twinning, which plays a key role in the deformation of magnesium alloys [39,40]. The twin boundary is interrupted by many micro-steps, resulting in a step-line distributed interface decomposition. It is also known that interfacial separation plays an important role in mechanical properties, especially thermal stability of magnesium alloys. The separated structure is not sensitive to heat treatment temperature and time, and has four crystallographic structural factors including crystal types, atomic radius, interfacial energy, distribution of stress field [41-43]. In Mg-Ag alloys, because the atomic diameter of Ag is lower than Mg, it tends to split into dislocation cores. Therefore, dislocations cause interruption of the separation between interfaces in micro steps. With the increase in the Ag content and the effect of extrusion, the grains were thinned and accordingly (Fig. 4(c)), it was observed that the hardness value increased. The size and distribution of the secondary Mg-Ag phase was thought to cause the increase in the hardness of the investigated alloys. This situation can be explained by the increase of Mg_4Ag β phases and dendrite structure independent of the heat treatment state. Similar results reported by the study of (Tie et al.) [23] and (Liu et al.) [36].

Fractography has been performed after the tensile tests (Fig. 5), the fracture surfaces of the investigated tensile specimens showed brittle fracture after casting and ductile after extrusion. The brittle fracture of the casting specimens can be attributed to the larger grain structure of as-cast alloys. Due to the reduction of grain size after extrusion, the fracture surface appearance has changed to ductile fracture with the formation of slip bands.

Corrosion of Mg-based implants causes four components: an abrasion surface on the implant; dissolved magnesium ions and other alloying elements; large amount of OH^-; and hydrogen gas. SBF solutions used in in vitro studies contain large amounts of buffering agents such as HCO^-3, $HPO4^{2-}$, Tris-HCl and Hepes, which can deplete the OH^- produced and mediate abrupt changes in pH [44]. Therefore, despite the rapid dissolution of magnesium in these buffered solutions, the pH changes slowly [44]. By the means of the given knowledge on these effects, the results of polarization and immersion tests on both pure Mg and Mg-Ag alloys have been analysed.

Three potentiodynamic polarization tests were made for each parameter and the average of the results found (Fig. 6-7) is given as a graphic.

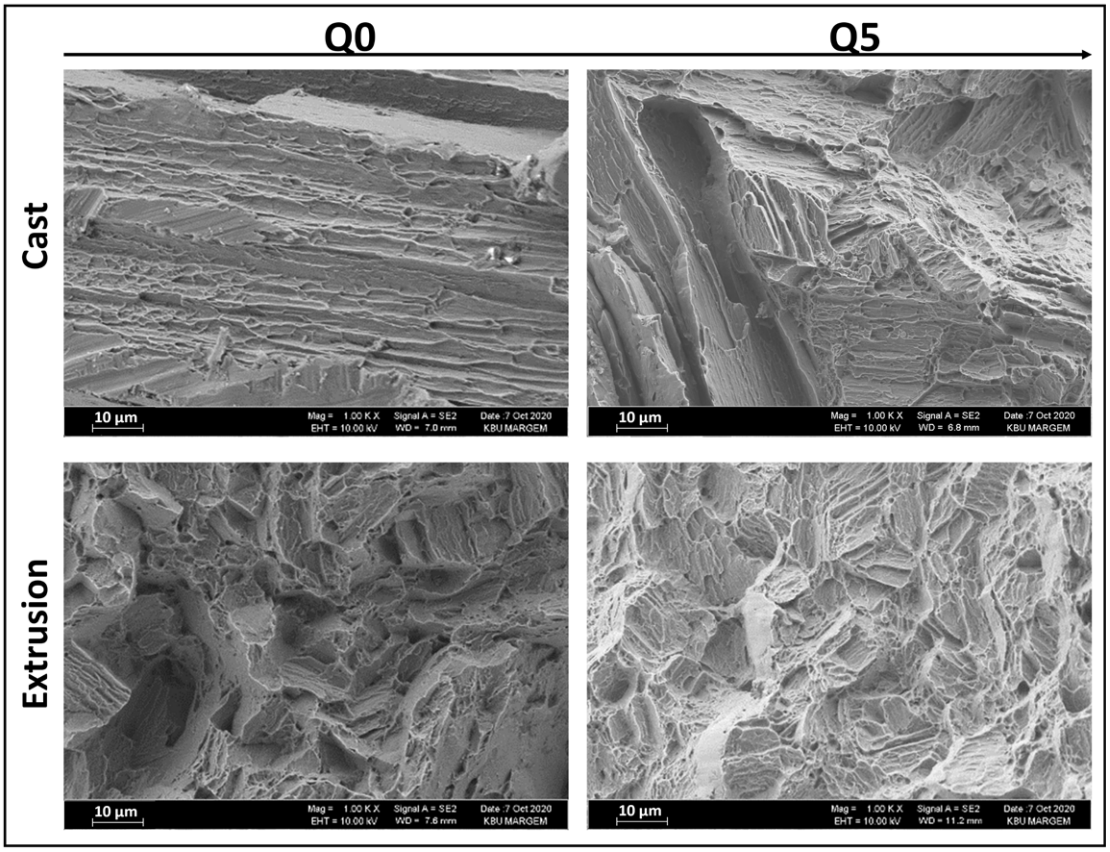

Fig. 5. Fracture surface analysis after tensile test

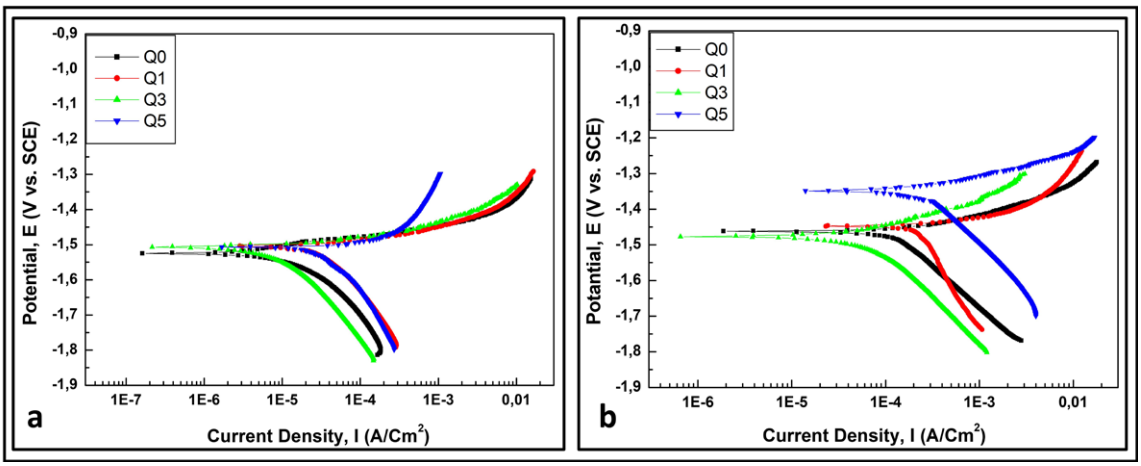

Fig. 6. Potentiodynamic polarization test results (a) after casting, (b) after extrusion

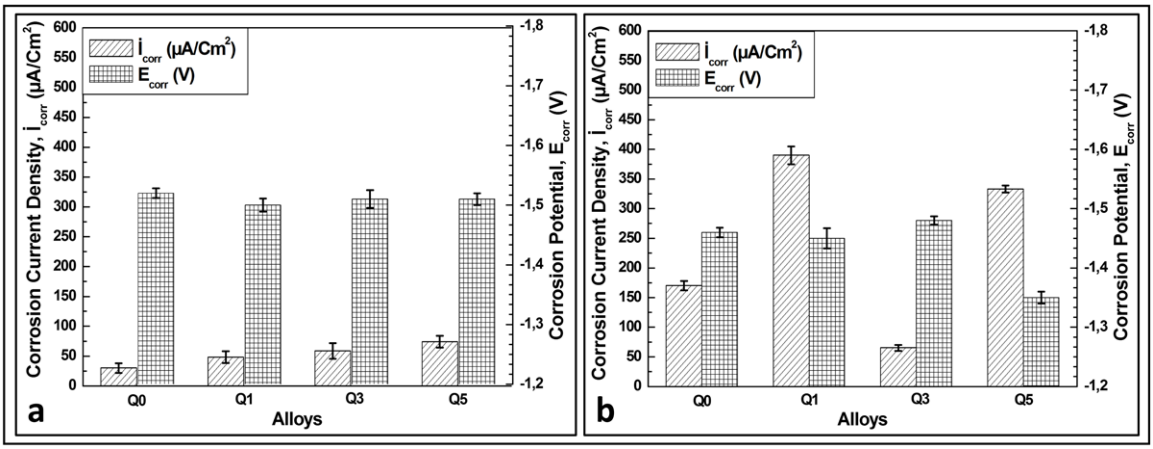

Fig. 7. Corrosion current density and potential values of alloys after (a) casting, (b) extrusion

As a result of the polarization tests, the examined corrosion current densities and corrosion potentials of the Ag containing alloys showed that the corrosion potential of the casting alloys was more negative than the corrosion potential of the extrusion alloys. The corrosion current density with Ag addition increased in the casting alloys. However, in the extruded alloys, the density decreased up to 3 wt. % Ag and increased with the addition of higher amount of Ag. According to the results obtained, the addition of Ag up to a certain amount (3 wt. %) and the extrusion process (for Q3 alloy) exhibited better corrosion properties. The increase in the corrosion current with 3 wt. % Ag amount might be based on the phases occurring in the microstructure being more noble than the Mg-matrix. Therefore they are acting as the cathode. In addition to that, with the application of the extrusion process, the volume fraction of the cathodic areas and the corrosion current density have increased. This case can be explained by the different distributions and sizes of the second phase particles. Thus, the discrete distribution of spherical-shaped $Mg_{54}Ag_{17}$ particles (Fig. 3) in the transverse direction formed a greater contact surface area with the matrix phase and possibly caused a stronger micro galvanic corrosion [45]. For this reason, it is thought that as a result of the extrusion process applied to the alloys, both the corrosion current density and the corrosion potential increased. However, the Q1 alloy containing 1 wt. % Ag exhibited very poor corrosion properties. (Zhao et al.) [46] reported in their study that the addition of Ag up to 1 wt. % provides poor corrosion resistance.

According to the galvanic corrosion principles, the fact that the α-Mg (anode phase) ratio is higher than the intermetallic (cathode phase) ratio plays an accelerating role in galvanic corrosion [13]. However, precipitations and segregations in materials often occur at the grain boundaries. Therefore, because of a) the secondary phases precipitate primarily and in large amounts along the grain boundaries, b) the increasing intermetallic phases with the Ag addition, c) the spreading secondary phases after homogenization into the grain as well as the grain boundaries, and (d) as a result of extrusion, the elongated grains in the structure (Fig. 7(b)), different corrosion rates were observed in this study. In addition, whether the dissolving effect of the secondary phases of homogenization (420°C 12 hours) process is the same in all alloys can be examined as another study issue with diffusion control.

Immersion test results of the cast and extruded alloys containing pure-Mg and 1-5 wt. % Ag are given in Fig. 8. Fig. 8 shows, apart for alloy Q5, that the corrosion rate loss of the cast alloys is lower than that of the extruded alloys. Since the protec-

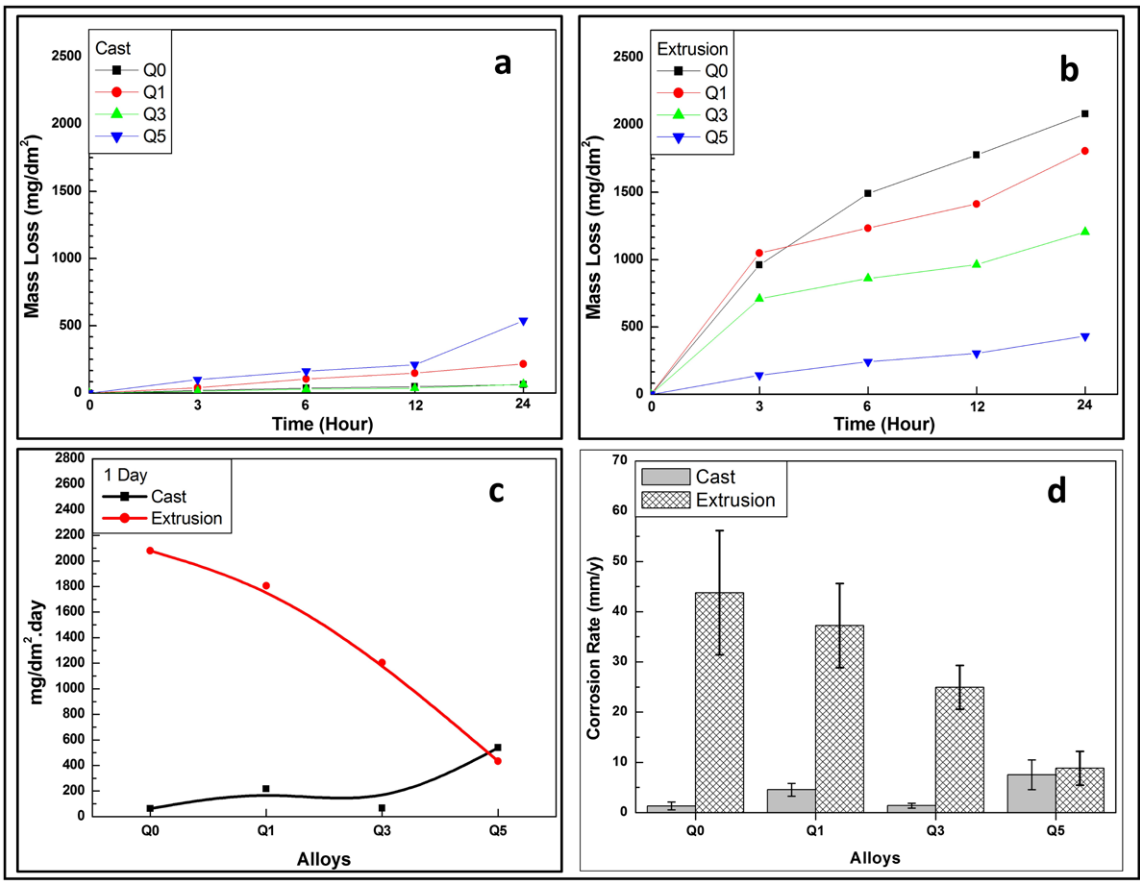

Fig. 8. After the immersion test in the Hanks solution, mass loss of (a) the cast and (b) extruded samples according to time and (c) corrosion rate of the cast and extruded samples (d) corrosion rate (mm/y) of Q0 and Q5 after immersion in the conditions: as-cast and extruded

tive oxide film layer formed on the surface of magnesium is less stable than the oxide layer of many metals, it cannot be effective in deactivating the corrosion progress at the first onset of corrosion [11]. Because of this metastable oxide layer, magnesium alloys primarily exhibit rapid dissolution in corrosive media. With dissolution, the oxide film layer on the surface becomes more stable and dissolution slows down due to corrosion effect. However, Ag has a great influence on the degradation behavior of the Mg-xAg alloys. Since it has low solubility in magnesium at ambient temperature [47], when the Ag content is higher, there is more secondary phase or precipitate in Mg-Ag alloys [23]. Thus, both the amount and distribution of precipitate may affect the degradation behavior depending on the microgalvanic corrosion principle [48-50]. The corrosion rate increases linearly with increasing amounts of sediment, and precipitates can cause a local degradation state [51].Therefore, the corrosion rates of the extruded alloys decreased with the addition of Ag, whereas the opposite results have occurred in the casting alloys. (Bryla at al.) [52] and (Yang at al.) [53] observed a similar situation in their study and reported that the corrosion rates of Mg-Ag casting alloys were higher. The mean corrosion rate CR_m was calculated according to Eq. (1) and is shown in Fig. 8(d). It was observed that it increased as the Ag addition increased (Q3 except) in as-cast alloys. But opposite case was observed in extruded alloys. Both the corrosion rates of the extruded and that of the cast Q5 alloys are similar.

After the immersion corrosion test, the visual inspection showed that the corrosive surface of the Q0 alloy was almost completely white, while black corrosion layers containing various sized white precipitates were observed in the cast alloys with Ag additions. However, the opposite situation was observed after the corrosion tests of the extruded alloys. It was observed that the outer corrosion layers of the samples were mainly composed of MgO/Mg $(OH)_2$. The different appearances on the surface are formed by the different density and thickness of corrosion products.

Fig. 9 shows the representative morphologies of the corroded areas of the cross-sections for both Q0 and Q5 alloys. According to results, pits found in the Q0 samples are the more in the extruded rather than the as-cast, of a high amount and shaped as subsurface or undercutting pits (Fig. 9), whereas in Q5 they were observed in the as-cast more than extruded alloy. In addition pits were observed, both in the direction perpendicular and in the direction parallel to the extrusion direction in the Q5 alloy. But these pits do not appear to be in a critical narrow and very deep shape in the all alloys.

Fig. 10 shows the pitting factors of the alloys Q0 and Q5 and their dependence on the extrusion and Ag include condition. Q0 as-cast is shown pitting factor around 1,2. This is the highest pitting factor. Because with a lower corrosion rate as a result of passivation (see Fig. 8) the pitting factor increases when the oxide layer is obviously not dense enough, which agrees with

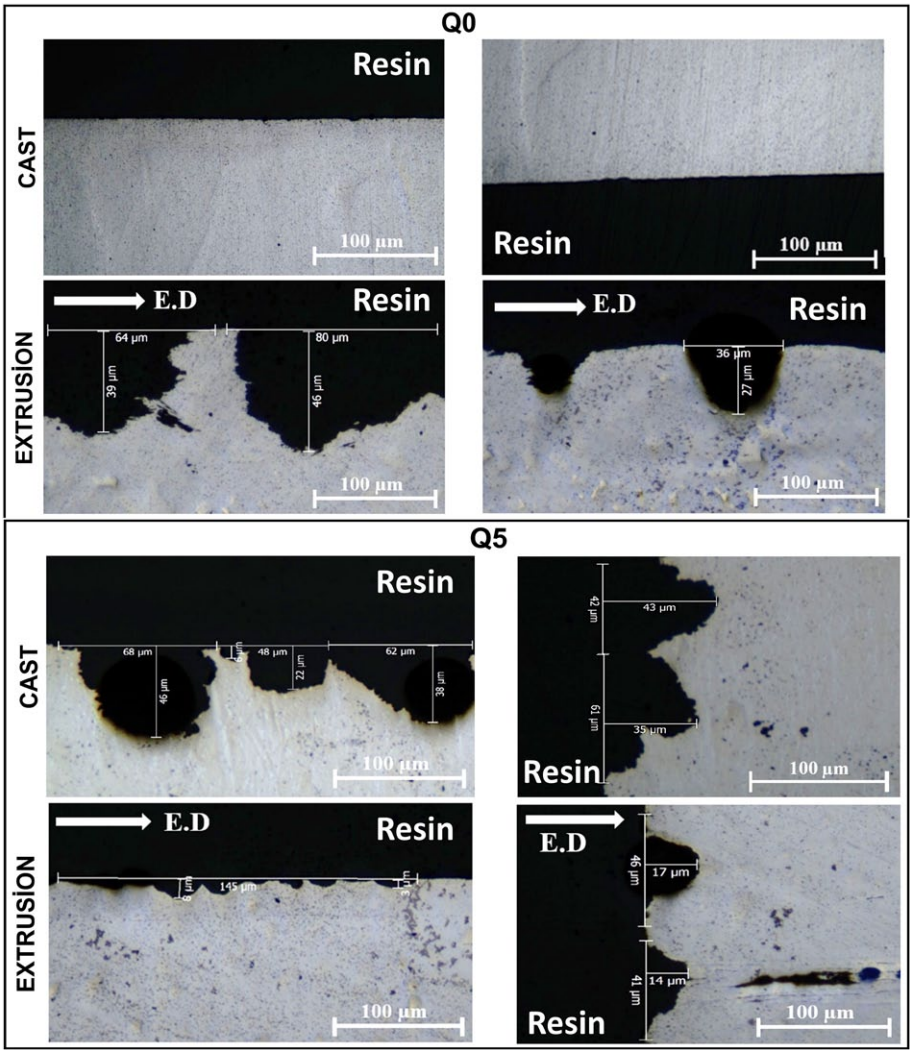

Fig. 9. Cross-sectional micrographs showing corrosion morphology of Q0 and Q5

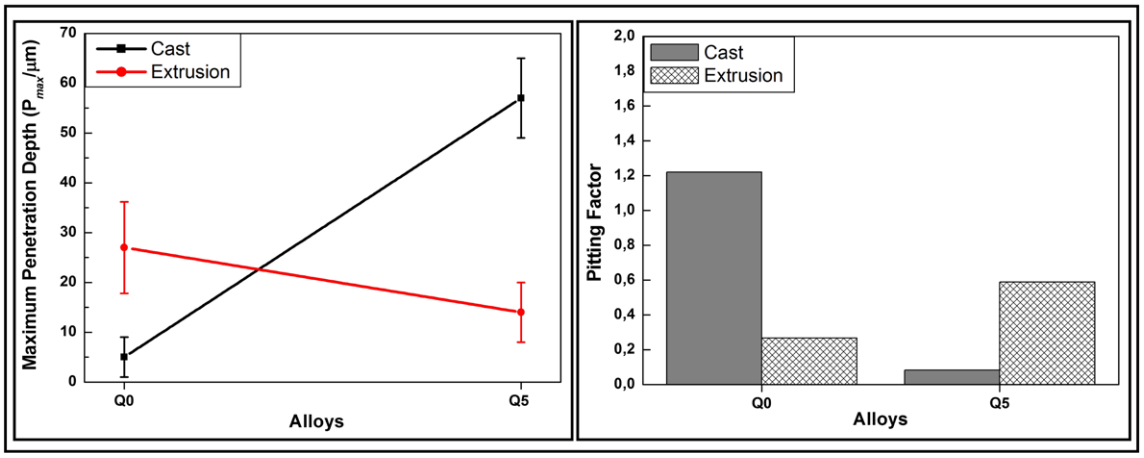

Fig. 10. Pitting factor and maximum penetration depth (P_{max}) of Q0 and Q5 alloys

the immersion tests [54]. However, pitting factor is the lowest in the as-cast Q5 alloy.

SEM and EDX analysis after the immersion corrosion test are given in Fig. 11. With respect to Fig. 11, the corrosion appearance of the examined cast samples containing 5 wt. % Ag exhibited a porous oxide appearance, while that of the extruded samples gained a flat and non-porous oxide appearance with the addition of 5 wt. % Ag.

Corrosion rate, wear rates and average friction coefficients obtained as a result of wear test of the cast and extruded alloys are given. In Fig. 12, it is known that simulated body fluids have some effects on the wear behavior of magnesium alloys.

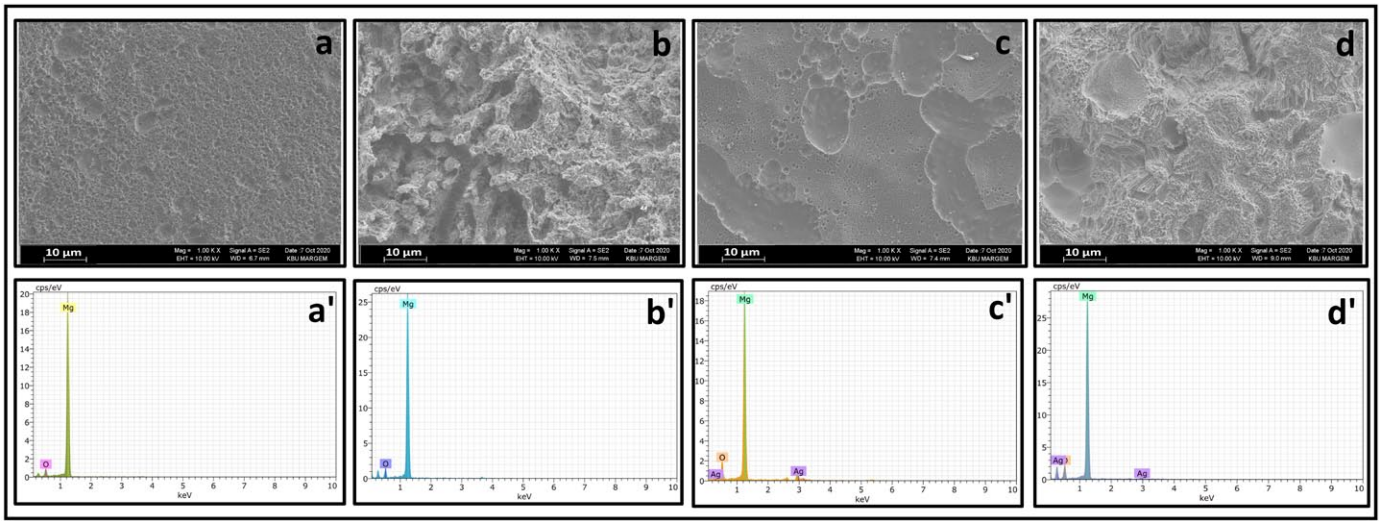

Fig. 11. SEM images and EDX Analysis of the corroded (a) Q0, (b) Q5 Cast and (c) Q0, (d) Q5 extruded samples

The graphs show that grain refinement of the α-Mg and secondary phases due to the extrusion process increased the hardness and prevented the progress of corrosive wear, resulting in less mass loss.

The corrosion effect of Hanks solution makes the surface of the cast magnesium alloy loose and porous, causing it to wear out more easily. At the same time, magnesium alloy is vulnerable to scratching under high load generally, causing the alloy to corrode easily. The two influencing factors act simultaneously on the magnesium alloy and exacerbate the corrosive wear of the magnesium alloy. In the literature [12, 55] the wear rate and the friction coefficient have generally been similar to each other, as a load of 2-10 N has been applied. However, due to the amount of load applied and sliding distance in this study were 20 N and 400 m, different results were obtained in the current coefficient and wear rate (Fig. 12(c), (d)) on the contrary reported in the Ref. [12,55].

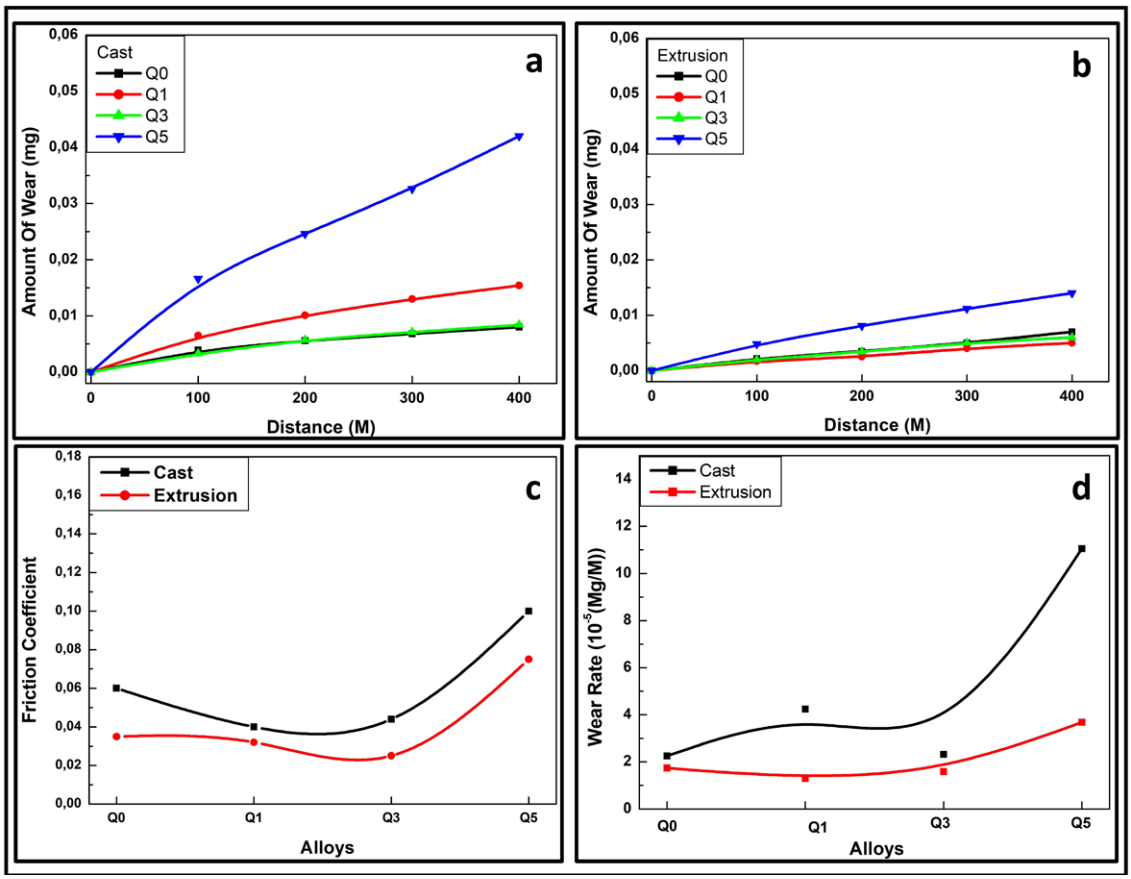

Fig. 12. After wear test in the Hanks solution, mass loss of (a) the cast samples and (b) the extruded samples according to distance, (c) friction coefficients of the cast and extruded samples, (d) wear rates of the cast and extruded samples

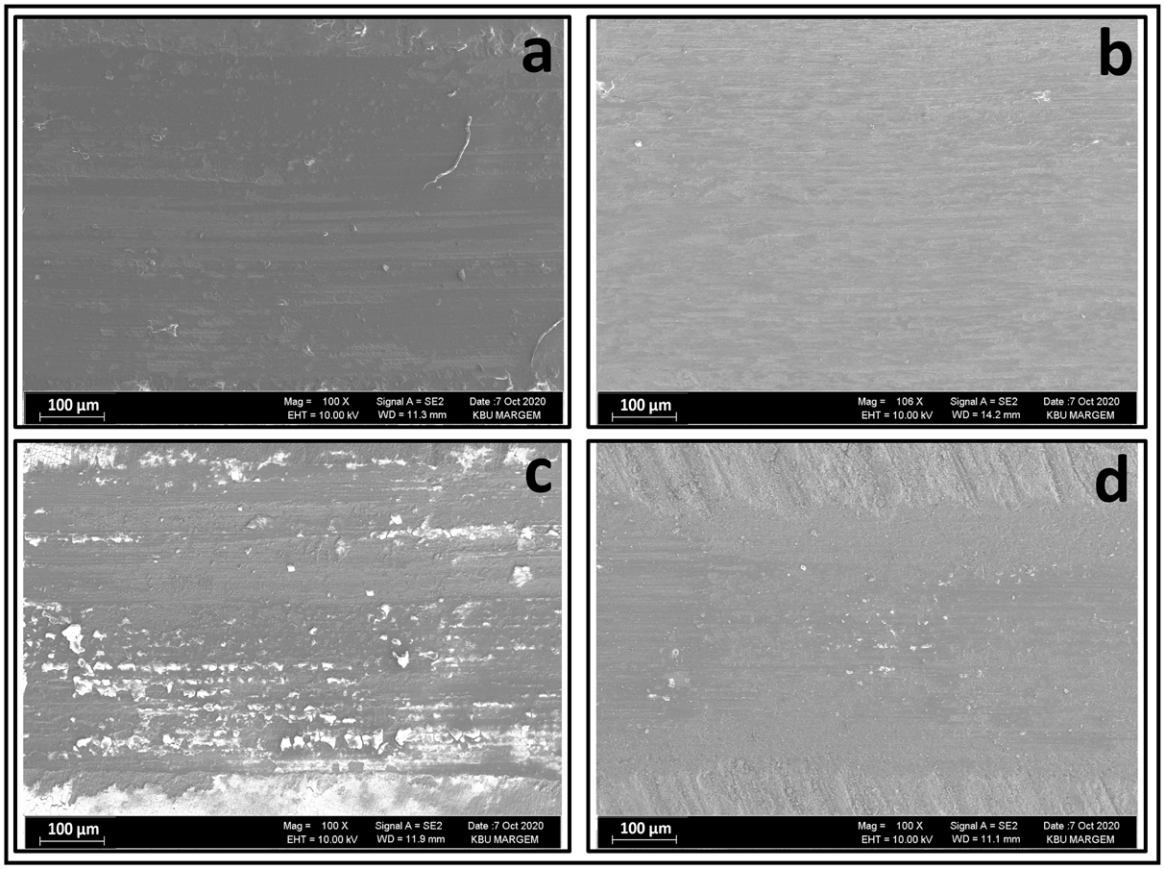

Fig. 13. SEM images of the corrosive wear test applied to alloys after (a) Q0, (b) Q5 casting and (c) Q0, (d) Q5 extrusion

In Fig. 13, SEM and EDX analysis of wear surfaces after corrosive wear test are given. The surface of the cast magnesium alloy worn in the Hanks solution becomes coated loose flakes and is easily worn. At the same time, the magnesium alloy corrodes easily, as it has poor scratch resistance under high load. These two influencing factors occur simultaneously on the magnesium alloy and exacerbate the corrosion of the magnesium alloy. With the increase in Ag addition, casting alloys have weaker scratch resistance. However, with the extrusion process, wear resistance and corrosion resistance can be increased.

4. Conclusions

Following main findings of this study can be summarized:

1. With the increase of the amount of Ag added to Mg, the higher presence of Mg_4Ag and $Mg_{54}Ag_{17}$ phases were detected in the microstructure.
2. Compared to pure magnesium, it has been determined that the grain size decreases with the addition of Ag and thus, better mechanical properties appear.
3. It has been observed that tensile and yield stress and % elongation increase due to the refinement of the microstructure by the extrusion process as well as the Ag addition.
4. By potentiodynamic polarization tests, it has been determined that up to 5 wt. % Ag addition and extrusion process (for Q5 alloy) exhibit better corrosion properties. The Q1 alloy, on the other hand, was found to have very poor corrosion properties.
5. When the results of the immersion corrosion tests are examined, it has been determined that the weight loss in all cast alloys is almost constant in the first 3-12 hours of immersion, and after these hours, Q1 and Q5 alloys progress faster.
6. In all of the extruded alloys, it was observed that the mass loss was lower as a result of the extrusion process thinning the α-Mg and secondary phases more, and consequently, the increase in hardness and the fine-grained microstructure preventing corrosion from progressing.

Acknowledgment

This research is supported by The Scientific And Technological Research Council Of Turkey (TUBITAK) with1002 - Short Term R&D Funding Program, project no 119M645.

REFERENCES

[1] S. Zhang, X. Zhang, C. Zhao, J. Li, Y. Song, C. Xie, H. Tao, Y. Zhang, Y. He, Y. Jiang, Acta Biomater. **6** (2), 626-640 (2010). DOI: https://doi.org/10.1016/j.actbio.2009.06.028

[2] X. Zhang, G. Yuan, J. Niu, P. Fu, W. Ding, J. Mech. Behav. Biomed. Mater. **9**, 153-162 (2012). DOI: https://doi.org/10.1016/j.jmbbm.2012.02.002

[3] Z. Li, X. Gu, S. Lou, Y. Zheng, Biomaterials **29** (10), 1329-1344 (2008). DOI: https://doi.org/0.1016/j.biomaterials.2007.12.021

[4] G. Song, S. Song, Adv. Eng. Mater. **9** (4), 298-302 (2007). DOI: https://doi.org/10.1002/adem.200600252

[5] M.P. Staiger, A.M. Pietak, J. Huadmai, G. Dias, Biomaterials **27** (9), 1728-1734 (2006). DOI: https://doi.org/10.1016/j.biomaterials.2005.10.003

[6] A. Purnama, H. Hermawan, J. Couet, D. Mantovani, Acta Biomater. **6** (5), 1800-1807 (2010). DOI: https://doi.org/10.1016/j.actbio.2010.02.027

[7] C.M. Agrawal, JOM **50** (1), 31-35 (1998). DOI: https://doi.org/10.1007/s11837-998-0064-5

[8] J. Nagels, M. Stokdijk, P.M. Rozing, J. Shoulder Elbow Surg. **12** (1), 35-39 (2003). DOI: https://doi.org/10.1067/mse.2003.22

[9] M. Salahshoor, Y. Guo, Materials **5** (1), 135-155 (2012). DOI: https://doi.org/10.3390/ma5010135

[10] F. Witte, H. Ulrich, M. Rudert, E. Willbold, J. Biomed. Mater. Res. A **81A** (3), 748-756 (2007). DOI: https://doi.org/10.1002/jbm.a.31170

[11] A. Atrens, G.-L. Song, F. Cao, Z. Shi, P.K. Bowen, J. Magnes. Alloys **1** (3), 177-200 (2013). DOI: https://doi.org/10.1016/j.jma.2013.09.003

[12] H. Li, D. Liu, Y. Zhao, F. Jin, and M. Chen, J. Mater. Eng. Perform. **25** (9), 3890-3895 (2016). DOI: https://doi.org/10.1007/s11665-016-2207-0

[13] G.L. Song, A. Atrens, Adv. Eng. Mater. **1** (1), 11-33 (1999). DOI: https://doi.org/10.1002/(SICI)1527-2648(199909)1:1<11::AID-ADEM11>3.0.CO;2-N

[14] R. Zeng, J. Zhang, W. Huang, W. Dietzel, K.U. Kainer, C. Blawert, W. Ke, Trans. Nonferrous Met. Soc. China **16**, s763-s771 (2006). DOI: https://doi.org/10.1016/S1003-6326(06)60297-5

[15] E. Koç, M.B. Kannan, M. Ünal, E. Candan, J. Alloys Compd. **648**, 291-296 (2015). DOI: https://doi.org/10.1016/j.jallcom.2015.06.227

[16] İ.H. Kara, H. Ahlatçı, Y. Türen, Y. Sun, Arab. J. Geosci. **11** (18), 535 (2018). DOI: https://doi.org/10.1007/s12517-018-3871-1

[17] E. Koc, M. Unal, Y. Turen, H.A. Goren, E. Candan, Int. J. Mater. Sci. Appl. **7** (1), 13 (2018). DOI: https://doi.org/10.11648/j.ijmsa.20180701.13

[18] H.A. Gören, M. Ünal, E. Koç, Acta Phys. Pol. A **135** (5), 884-887 (2019). DOI: https://doi.org/10.12693/APhysPolA.135.884

[19] H. Zengin, Y. Turen, L. Elen, J. Mater. Eng. Perform. **28** (8), 4647-4657 (2019). DOI: https://doi.org/10.1007/s11665-019-04223-8

[20] L. Elen, B. Cicek, E. Koc, Y. Turen, Y. Sun, H. Ahlatci, Mater. Res. Express **6** (9), (2019). DOI: https://doi.org/10.1088/2053-1591/ab2b13

[21] H. Zengin, Y. Turen, H. Ahlatci, Y. Sun, A.C. Karaoğlanli, Trans. Nonferrous Met. Soc. China **29** (7), 1413-1423 (2019). DOI: https://doi.org/10.1016/S1003-6326(19)65048-X

[22] Y. Zheng, Magnesium alloys as degradable biomaterials, CRC Press, Taylor & Francis Group, Boca Raton London New York (2015).

[23] D. Tie, F. Feyerabend, W.-D. Müller, R. Schade, K. Liefeith, K. Kainer, R. Willumeit, Eur. Cell. Mater. **25**, 284-298 (2013). DOI: https://doi.org/10.22203/eCM.v025a20

[24] J. Hardes, A. Streitburger, H. Ahrens, T. Nusselt, C. Gebert, W. Winkelmann, A. Battmann, G. Gosheger, Sarcoma **2007**, 26539 (2007). DOI: https://doi.org/10.1155/2007/26539

[25] M. Bosetti, A. Massè, E. Tobin, M. Cannas, Biomaterials **23** (3), 887-892 (2002). DOI: https://doi.org/10.1016/s0142-9612(01)00198-3

[26] ATSDR, (1990).

[27] A. Furst, M.C. Schlauder, J. Environ. Pathol. Toxicol. **1** (1), 51-57 (1978).

[28] I. Nakatsugawa, N. Saito, K. Suzuki, Y. Chino, Y. Fukuda, T. Ito, M. Noda, Y. Gonda, Mater. Trans. **61** (9), 1798-1804 (2020). DOI: https://doi.org/10.2320/matertrans.L-M2020839

[29] H.M. Wong, Y. Zhao, V. Tam, S. Wu, P.K. Chu, Y. Zheng, M.K.T. To, F.K.L. Leung, K.D.K. Luk, K.M.C. Cheung, K.W.K. Yeung, Biomaterials **34** (38), 9863-9876 (2013). DOI: https://doi.org/10.1016/j.biomaterials.2013.08.052

[30] Y. Dai, H. Liu, Y. Tang, X. Xu, H. Long, Y. Yan, Z. Luo, Y. Zhang, K. Yu, Y. Zhu, Metals **8** (11), 948 (2018). DOI: https://doi.org/10.3390/met8110948

[31] D. Tie, F. Feyerabend, N. Hort, D. Hoeche, K.U. Kainer, R. Willumeit, W.D. Mueller, Mater. Corros. **65** (6), 569-576 (2014). DOI: https://doi.org/10.1002/maco.201206903

[32] K. Yu, Y. Dai, Z. Luo, H. Long, M. Zeng, Z. Li, J. Zhu, L. Cheng, Y. Zhang, H. Liu, Y. Zhu, J. Biomed. Mater. Res. A **106** (7), 2059-2069 (2018). DOI: https://doi.org/10.1002/jbm.a.36397

[33] Z. Zhao, Q. Chen, H. Chao, S. Huang, Mater. Des. **31** (4), 1906-1916 (2010). DOI: https://doi.org/10.1016/j.matdes.2009.10.056

[34] H. Zengin, Investigation Of The Effect Of Alloying Elements On Mechanical And Corrosion Properties Of ZK60 Magnesium Alloys After Casting And Extrusion, Ph. D. Thesis, Karabuk University, Karabuk 78050, September

[35] Y. Uematsu, K. Tokaji, M. Kamakura, K. Uchida, H. Shibata, N. Bekku, Mater. Sci. Eng. A **434** (1), 131-140 (2006). DOI: https://doi.org/10.1016/j.msea.2006.06.117

[36] Z. Liu, F. Feyerabend, R. Willumeit, Mechanical properties of extruded antimicrobial Mg-Ag alloys, in:, p. 14 (2014).

[37] Y. Estrin, N. Martynenko, N. Anisimova, D. Temralieva, M. Kiselevskiy, V. Serebryany, G. Raab, B. Straumal, B. Wiese, R. Willumeit-Römer, S. Dobatkin, Materials **12** (23), 3832 (2019). DOI: https://doi.org/10.3390/ma12233832

[38] Y. Liu, X. Chen, K. Wei, L. Xiao, B. Chen, H. Long, Y. Yu, Z. Hu, H. Zhou, Mater. Basel Switz. **12** (8), (2019). DOI: https://doi.org/10.3390/ma12081307

[39] H. Wang, P.D. Wu, J. Wang, C.N. Tomé, Int. J. Plast. **49**, 36-52 (2013). DOI: 10.1016/j.ijplas.2013.02.016

[40] X. Liao, J. Wang, J. Nie, Y. Jiang, P. Wu, MRS Bull. **41** (4), 314-319 (2016). DOI: https://doi.org/10.1557/mrs.2016.64

[41] H. Zhou, G.M. Cheng, X.L. Ma, W.Z. Xu, S.N. Mathaudhu, Q.D. Wang, Y.T. Zhu, Acta Mater. **95**, 20-29 (2015). DOI: https://doi.org/10.1016/j.actamat.2015.05.020

[42] L.R. Xiao, Y. Cao, S. Li, H. Zhou, X.L. Ma, L. Mao, X.C. Sha, Q.D. Wang, Y.T. Zhu, X.D. Han, Acta Mater. **162**, 214-225 (2019). DOI: https://doi.org/10.1016/j.actamat.2018.10.005

[43] J.F. Nie, Y.M. Zhu, J.Z. Liu, X.Y. Fang, Science **340** (6135), 957-960 (2013). DOI: https://doi.org/10.1126/science.1229369

[44] Y. Xin, T. Hu, P.K. Chu, Acta Biomater. **7** (4), 1452-1459 (2011). DOI: https://doi.org/10.1016/j.actbio.2010.12.004

[45] H. Zengin, Y. Turen, J. Magnes. Alloys **8** (3), 640-653 (2020). DOI: https://doi.org/10.1016/j.jma.2020.06.004

[46] H. Zhao, L.-Q. Wang, Y.-P. Ren, B. Yang, S. Li, G.-W. Qin, Acta Metall. Sin. Engl. Lett. **31** (6), 575-583 (2018). DOI: https://doi.org/10.1007/s40195-018-0712-x

[47] A.A. Nayeb-Hashemi, J.B. Clark, Bull. Alloy Phase Diagr. **5** (4), 348 (1984). DOI: https://doi.org/10.1007/BF02872949

[48] G. Song, A. Atrens, Adv. Eng. Mater. **5** (12), 837-858 (2003). DOI: https://doi.org/10.1002/adem.200310405

[49] F. Witte, N. Hort, C. Vogt, S. Cohen, K.U. Kainer, R. Willumeit, F. Feyerabend, Curr. Opin. Solid State Mater. Sci. **12** (5), 63-72 (2008). DOI: https://doi.org/10.1016/j.cossms.2009.04.001

[50] J. Bohlen, S. Meyer, B. Wiese, B.J.C. Luthringer-Feyerabend, R. Willumeit-Römer, D. Letzig, Materials **13** (2), 391 (2020). DOI: https://doi.org/10.3390/ma13020391

[51] E. Ghali, W. Dietzel, K.-U. Kainer, J. Mater. Eng. Perform. **13** (1), 7-23 (2004). DOI: https://doi.org/10.1361/10599490417533

[52] K. Bryła, J. Horky, M. Krystian, L. Lityńska-Dobrzyńska, B. Mingler, Mater. Sci. Eng. C **109**, 110543 (2020). DOI: https://doi.org/10.1016/j.msec.2019.110543

[53] L. Yang, Y. Shi, L. Shen, E. Zhang, G. Qin, X. Lu, X. Zhou, Corros. Sci. **185**, 109408 (2021). DOI: https://doi.org/10.1016/j.corsci.2021.109408

[54] P. Maier, N. Lauth, C.L. Mendis, M. Bechly, N. Hort, JOM **71** (4), 1426-1435 (2019). DOI: https://doi.org/10.1007/s11837-019-03359-1

[55] D.-B. Liu, B. Wu, X. Wang, M.-F. Chen, Rare Met. **34** (8), 553-559 (2015). DOI: https://doi.org/10.1007/s12598-013-0052-y